RESEARCH ARTICLE

Bifurcation analysis of nonlinear time-periodic time-delay systems via semidiscretization

T. G. Molnar[1] | Z. Dombovari[1] | T. Insperger[2] | G. Stepan[1]

[1]Department of Applied Mechanics, Budapest University of Technology and Economics, Budapest, Hungary

[2]Department of Applied Mechanics, Budapest University of Technology and Economics and MTA-BME Lendület Human Balancing Research Group, Budapest, Hungary

Correspondence
T. G. Molnar, Department of Applied Mechanics, Budapest University of Technology and Economics, 1111 Budapest, Hungary.
Email: molnar@mm.bme.hu

Summary

Bifurcations of the periodic stationary solutions of nonlinear time-periodic time-delay dynamical systems are analyzed. The solution operator of the governing nonlinear delay-differential equation is approximated by a sequence of nonlinear maps via semidiscretization. The subsequent nonlinear maps are combined to a single resultant nonlinear map that describes the evolution over the time period. Fold, flip, and Neimark-Sacker bifurcations related to the fixed point of this map are analyzed via center manifold reduction and normal form theorems. The analysis unfolds the approximate stability properties and bifurcations of the stationary solution of the delay-differential equation and, at the same time, allows the approximate computation of the arising period-1, period-2, and quasi-periodic solution branches. The method is demonstrated for the delayed Mathieu-Duffing equation, and the results are verified by numerical continuation.

KEYWORDS

delay-differential equation, dynamical systems, nonlinear dynamics, semidiscretization, time-periodic systems

1 | INTRODUCTION

Bifurcation analysis of time-delay systems has been a frequently discussed research topic in the past few years. Several analytical approaches have been developed to investigate nonlinear delay-differential equations (DDEs), such as the center manifold reduction[1-3] and the method of multiple scales.[4] Due to the algebraic complexity of these methods, numerical approaches for stability and bifurcation analysis of DDEs have also gained ground. The most well-known computational tool is DDE-BIFTOOL,[5] which enables the continuation of bifurcations and branches of solutions in autonomous systems. DDE-BIFTOOL is also capable of computing critical normal form coefficients for different kinds of codimension-1 and codimension-2 bifurcations in autonomous DDEs. Other methods also allow numerical continuation for autonomous systems (see, eg, the work of Breda et al[6]); however, only a few techniques are dedicated to the analysis of time-periodic DDEs. The package KNUT[7,8] enables the continuation of bifurcations related to periodic solutions of time-periodic DDEs. However, the computation of critical normal form coefficients associated with these bifurcations is not implemented. To the authors' best knowledge, so far, the normal form analysis realized in DDE-BIFTOOL for autonomous DDEs has not been extended to time-periodic systems.

Here, we carry out approximate normal form analysis for time-periodic DDEs, by which the stability and bifurcations of the stationary periodic solution can be investigated. Our approach is based on discretizing the solution operator of

the nonlinear time-periodic DDE using a nonlinear map that describes the evolution over the time period. The fixed point of this map corresponds to the stationary solution of the original DDE. Fold, flip, and Neimark-Sacker bifurcations of the fixed point are associated with cyclic fold, period doubling, and secondary Hopf bifurcations of the stationary solution, respectively, which may give rise to period-1, period-2, and quasi-periodic solutions. We determine the stability of these solutions by analyzing the fixed point of the corresponding nonlinear map and calculating its critical normal form coefficients. Via these coefficients, we use analytical formulas to obtain the approximate amplitude of the bifurcating solutions as a function of the bifurcation parameter. Therefore, as opposed to KNUT, this method does not require the point-by-point continuation of the arising solutions; however, the results are accurate in the vicinity of the bifurcation point only, and secondary bifurcations cannot be detected.

The first step of the analysis is to discretize the solution operator of the nonlinear time-periodic DDE. Several techniques exist for discretizing DDEs (see the works of Krauskopf et al,[9] Loiseau et al,[10] and Breda et al[11] where some relevant approaches are collected). The most popular and most efficient numerical methods include the pseudospectral collocation,[12,13] the Chebyshev spectral continuous-time approximation,[14] the spectral element method,[15] the spectral Legendre tau method,[16] and the pseudospectral tau method.[17] In what follows, we use the semidiscretization technique[18] to discretize the solution operator of the DDE. This method formulates a sequence of nonlinear maps that approximate the dynamics over the time period. Note that the approach of this paper is not restricted to semidiscretization; it supports other discretization techniques as well, as long as the solution operator is approximated by a (sequence of) nonlinear map(s) over the time period.

We show an algorithm to build a single resultant map from the sequence of nonlinear maps that is correct up to third order in terms of the state variables. The bifurcation analysis of the resultant map is performed according to the bifurcation theory of discrete maps discussed in the works of Guckenheimer and Holmes[19] and Kuznetsov.[20] In the work of Kuznetsov,[20] center manifold reduction is used to reduce the dimension of maps in the vicinity of the bifurcation point. Thereby, closed-form formulas are given in the aforementioned work[20] for the critical normal form coefficients of maps where the fixed point undergoes fold, flip, or Neimark-Sacker bifurcation. These normal form coefficients can be used to analyze the bifurcation scenario in the original time-periodic DDE and to determine the stability and the approximate amplitude of solutions arising from cyclic fold, period doubling, and secondary Hopf bifurcations, respectively.

The rest of this paper is organized as follows. Section 2 presents the semidiscretization for nonlinear time-periodic DDEs. This results in a sequence of maps that is combined to a single resultant nonlinear map in Section 3. Bifurcation analysis of the resultant map is presented Section 4, where the normal form coefficients of fold, flip, and Neimark-Sacker bifurcations are given. Section 5 demonstrates the analysis of the delayed Mathieu-Duffing equation as a representative example, and conclusions are drawn in Section 6.

2 | THE TIME-PERIODIC SYSTEM AND ITS DISCRETIZATION

2.1 | Governing equation

In this paper, we investigate nonlinear time-periodic time-delay systems of the form

$$\dot{\mathbf{y}}(t) = \mathbf{f}(t, \mathbf{y}(t), \mathbf{y}(t - \tau)), \tag{1}$$

where $\mathbf{y} \in \mathbb{R}^n$. The function $\mathbf{f} : \mathbb{R}^+ \times \mathbb{R}^n \times \mathbb{R}^n \to \mathbb{R}^n$ is smooth in its second and third arguments and periodic in its first argument, ie, $\mathbf{f}(t, ., .) = \mathbf{f}(t + T, ., .)$, where T is the time period. We assume that Equation (1) has a time-periodic (stationary) solution $\mathbf{y}_\mathrm{p}(t) = \mathbf{y}_\mathrm{p}(t + T)$, and we are interested in the bifurcation of this solution. Therefore, we decompose the solution $\mathbf{y}(t)$ into the sum of the stationary solution $\mathbf{y}_\mathrm{p}(t)$ and a perturbation $\mathbf{u}(t)$ as $\mathbf{y}(t) = \mathbf{y}_\mathrm{p}(t) + \mathbf{u}(t)$. We can write the variational system corresponding to Equation (1) in the form[21]

$$\dot{\mathbf{u}}(t) = \mathbf{D}(t)\mathbf{u}(t) + \mathbf{E}(t)\mathbf{u}(t - \tau) + \mathbf{g}(t, \mathbf{u}(t), \mathbf{u}(t - \tau)), \tag{2}$$

where $\mathbf{D}(t), \mathbf{E}(t) \in \mathbb{R}^{n \times n}$, $\mathbf{D}(t) = \mathbf{D}(t + T)$, and $\mathbf{E}(t) = \mathbf{E}(t + T)$ are the coefficient matrices of the actual and retarded linear terms, respectively, and $\mathbf{g} : \mathbb{R}^+ \times \mathbb{R}^n \times \mathbb{R}^n \to \mathbb{R}^n$ represents the nonlinearities such that $\mathbf{g}(t, ., .) = \mathbf{g}(t + T, ., .)$ and $\mathbf{g}(t, \mathbf{0}, \mathbf{0}) \equiv \mathbf{0}$. Note that $\mathbf{u}(t) \equiv \mathbf{0}$ is the trivial solution of Equation (2), and the bifurcation analysis of $\mathbf{y}_\mathrm{p}(t)$ is equivalent to the analysis of the trivial solution $\mathbf{u}(t) \equiv \mathbf{0}$.

2.2 │ Semidiscretization

Here, we conduct the bifurcation analysis numerically via the semidiscretization technique.[18] By the discretization of the solution operator, semidiscretization resolves the time period T into $p \in \mathbb{N}^+$ steps and considers the flow between the time instants $t_k = k\Delta t$, where $k = 0, 1, \ldots, p$ and $\Delta t = T/p$. The time-periodic terms are approximated in this case by constants during each time step; thus, Equation (2) is approximated by

$$\dot{\mathbf{u}}(t) = \mathbf{D}_k \mathbf{u}(t) + \mathbf{E}_k \mathbf{u}(t - \tau) + \mathbf{g}_k(\mathbf{u}(t), \mathbf{u}(t - \tau)), \quad t \in [t_k, t_{k+1}), \tag{3}$$

with

$$\mathbf{D}_k = \frac{1}{\Delta t} \int_{t_k}^{t_{k+1}} \mathbf{D}(t)\mathrm{d}t, \quad \mathbf{E}_k = \frac{1}{\Delta t} \int_{t_k}^{t_{k+1}} \mathbf{E}(t)\mathrm{d}t, \quad \mathbf{g}_k(., .) = \frac{1}{\Delta t} \int_{t_k}^{t_{k+1}} \mathbf{g}(t, ., .)\mathrm{d}t. \tag{4}$$

Consider first the zeroth-order semidiscretization. The nonlinear and the time-delay terms are also approximated by constants over the discretization interval $[t_k, t_{k+1})$:

$$\dot{\mathbf{u}}(t) = \mathbf{D}_k \mathbf{u}(t) + \mathbf{E}_k \mathbf{u}_{k-r} + \mathbf{g}_k(\mathbf{u}_k, \mathbf{u}_{k-r}), \quad [t_k, t_{k+1}), \tag{5}$$

where $\mathbf{u}_k = \mathbf{u}(t_k)$ and $r = \lfloor \tau/\Delta t \rfloor$. The semidiscretized system (5) can be solved over $[t_k, t_{k+1})$, which yields

$$\mathbf{u}_{k+1} = \mathbf{P}_k \mathbf{u}_k + \mathbf{R}_k \mathbf{u}_{k-r} + \mathbf{h}_k(\mathbf{u}_k, \mathbf{u}_{k-r}), \tag{6}$$

where

$$\mathbf{P}_k = \mathrm{e}^{\mathbf{D}_k \Delta t}, \quad \mathbf{R}_k = \int_0^{\Delta t} \mathrm{e}^{\mathbf{D}_k(\Delta t - s)}\mathrm{d}s \ \mathbf{E}_k, \quad \mathbf{h}_k(., .) = \int_0^{\Delta t} \mathrm{e}^{\mathbf{D}_k(\Delta t - s)}\mathrm{d}s \ \mathbf{g}_k(., .). \tag{7}$$

If $\mathbf{D}_k^{-1}$ exists, then the integrals simplify to

$$\mathbf{R}_k = (\mathbf{P}_k - \mathbf{I})\mathbf{D}_k^{-1}\mathbf{E}_k, \quad \mathbf{h}_k(., .) = (\mathbf{P}_k - \mathbf{I})\mathbf{D}_k^{-1}\mathbf{g}_k(., .). \tag{8}$$

In what follows, we employ the first-order semidiscretization to the linear delayed term in Equation (3), which gives

$$\mathbf{u}_{k+1} = \mathbf{P}_k \mathbf{u}_k + \mathbf{R}_{k,0} \mathbf{u}_{k-r} + \mathbf{R}_{k,1} \mathbf{u}_{k-r+1} + \mathbf{h}_k(\mathbf{u}_k, \mathbf{u}_{k-r}), \tag{9}$$

where the coefficient matrices are given by

$$\begin{aligned}
\mathbf{R}_{k,0} &= \int_0^{\Delta t} \frac{\tau - (r-1)\Delta t - s}{\Delta t} \mathrm{e}^{\mathbf{D}_k(\Delta t - s)}\mathrm{d}s \ \mathbf{E}_k, \\
\mathbf{R}_{k,1} &= \int_0^{\Delta t} \frac{s - \tau + r\Delta t}{\Delta t} \mathrm{e}^{\mathbf{D}_k(\Delta t - s)}\mathrm{d}s \ \mathbf{E}_k
\end{aligned} \tag{10}$$

and can be simplified to

$$\begin{aligned}
\mathbf{R}_{k,0} &= \left(\mathbf{D}_k^{-1} + \frac{1}{\Delta t} \left(\mathbf{D}_k^{-2} - (\tau - (r-1)\Delta t)\mathbf{D}_k^{-1} \right) (\mathbf{I} - \mathbf{P}_k) \right) \mathbf{E}_k, \\
\mathbf{R}_{k,1} &= \left(-\mathbf{D}_k^{-1} + \frac{1}{\Delta t} \left(-\mathbf{D}_k^{-2} + (\tau - r\Delta t)\mathbf{D}_k^{-1} \right) (\mathbf{I} - \mathbf{P}_k) \right) \mathbf{E}_k
\end{aligned} \tag{11}$$

if $\mathbf{D}_k^{-1}$ exists (see the work of Insperger and Stépán[18]).

Finally, map (9) can be represented in the form

$$\mathbf{z}_{k+1} = \mathbf{J}_k \mathbf{z}_k + \mathbf{H}_k(\mathbf{z}_k), \tag{12}$$

with

$$\mathbf{z}_k = \begin{bmatrix} \mathbf{u}_k \\ \mathbf{u}_{k-1} \\ \vdots \\ \mathbf{u}_{k-r} \end{bmatrix}, \quad \mathbf{J}_k = \begin{bmatrix} \mathbf{P}_k & \mathbf{0} & \cdots & \mathbf{0} & \mathbf{R}_{k,1} & \mathbf{R}_{k,0} \\ \mathbf{I} & & \cdots & & \mathbf{0} & \mathbf{0} \\ \vdots & & \ddots & & \vdots & \vdots \\ \mathbf{0} & & \cdots & & \mathbf{I} & \mathbf{0} \end{bmatrix}, \quad \mathbf{H}_k(\mathbf{z}_k) = \begin{bmatrix} \mathbf{h}_k(\mathbf{u}_k, \mathbf{u}_{k-r}) \\ \mathbf{0} \\ \vdots \\ \mathbf{0} \end{bmatrix}, \tag{13}$$

where $\mathbf{I}$ and $\mathbf{0}$ denote identity and zero matrices, respectively. Note that $\mathbf{J}_k \mathbf{z}_k$ represents the linear term, and $\mathbf{H}_k(\mathbf{z}_k)$ is purely nonlinear satisfying $\mathbf{H}_k(\mathbf{0}) = \mathbf{0}$, which implies that $\mathbf{z} = \mathbf{0}$ is a fixed point of Equation (13).

3 | GOVERNING NONLINEAR MAP

Map (12) approximates the evolution of system (2) over the time interval $[t_k, t_{k+1}]$. Applying map (12) successively p times, we get the resultant map $\mathbf{z}_0 \to \mathbf{z}_p$ in the form

$$\mathbf{z}_p = \mathbf{F}(\mathbf{z}_0), \tag{14}$$

which represents the approximate evolution of system (2) over the whole period T. Therefore, we carry out the (approximate) bifurcation analysis of the periodic solution $\mathbf{y}_\mathrm{p}(t)$ by deriving map (14) and analyzing its fixed point $\mathbf{z} = \mathbf{0}$. This section is dedicated to the derivation of the approximation of map (14) that is correct up to third order in terms of $\mathbf{z}_0$ and is suitable for bifurcation analysis. The third-order approximation is of the form

$$\mathbf{z}_p = \mathbf{A}\mathbf{z}_0 + \frac{1}{2}\langle \mathbf{B}, \mathbf{z}_0, \mathbf{z}_0 \rangle + \frac{1}{6}\langle \mathbf{C}, \mathbf{z}_0, \mathbf{z}_0, \mathbf{z}_0 \rangle + \mathcal{O}\left(\|\mathbf{z}_0\|^4\right), \tag{15}$$

where $\mathbf{A}$, $\mathbf{B}$, and $\mathbf{C}$ are second-, third-, and fourth-order coefficient matrices of the linear, quadratic, and cubic terms, respectively, that are yet to be derived. Using index notation, these matrices read

$$\mathbf{A} = [A_{jl}] = \left[\partial_l F_j\big|_0\right], \quad \mathbf{B} = [B_{jlm}] = \left[\partial_l \partial_m F_j\big|_0\right], \quad \mathbf{C} = [C_{jlmq}] = \left[\partial_l \partial_m \partial_q F_j\big|_0\right], \tag{16}$$

where ∂_l represents the partial derivative with respect to the lth element of $\mathbf{z}_0$ and subscript 0 stands for the substitution $\mathbf{z}_0 = \mathbf{0}$. Operations $\langle .,. \rangle$ and $\langle .,.,. \rangle$ are defined as

$$\langle \mathbf{B}, \mathbf{x}, \mathbf{y} \rangle := \left[B_{jlm}x_l y_m\right], \quad \langle \mathbf{C}, \mathbf{x}, \mathbf{y}, \mathbf{z} \rangle := \left[C_{jlmq}x_l y_m z_q\right]. \tag{17}$$

Note that these operations are linear and satisfy the following properties:

$$\langle \mathbf{K}, \mathbf{x} + \mathbf{y}, \mathbf{u} + \mathbf{v} \rangle = \langle \mathbf{K}, \mathbf{x}, \mathbf{u} \rangle + \langle \mathbf{K}, \mathbf{x}, \mathbf{v} \rangle + \langle \mathbf{K}, \mathbf{y}, \mathbf{u} \rangle + \langle \mathbf{K}, \mathbf{y}, \mathbf{v} \rangle,$$

$$\langle \mathbf{K}, \mathbf{U}\mathbf{x}, \mathbf{V}\mathbf{y} \rangle = \langle\langle \mathbf{K}, \mathbf{U}, \mathbf{V} \rangle, \mathbf{x}, \mathbf{y} \rangle,$$

$$\mathbf{U}\langle \mathbf{K}, \mathbf{x}, \mathbf{y} \rangle = \langle \mathbf{U}\mathbf{K}, \mathbf{x}, \mathbf{y} \rangle,$$

$$\langle \mathbf{K}, \mathbf{U}\mathbf{x}, \langle \mathbf{S}, \mathbf{y}, \mathbf{z} \rangle \rangle = \langle\langle \mathbf{K}, \mathbf{U}, \mathbf{S} \rangle, \mathbf{x}, \mathbf{y}, \mathbf{z} \rangle,$$

$$\langle \mathbf{K}, \langle \mathbf{S}, \mathbf{x}, \mathbf{y} \rangle, \mathbf{U}\mathbf{z} \rangle = \langle\langle \mathbf{K}, \mathbf{S}, \mathbf{U} \rangle, \mathbf{x}, \mathbf{y}, \mathbf{z} \rangle, \tag{18}$$

$$\langle \mathbf{L}, \mathbf{x} + \mathbf{y}, \mathbf{z} + \mathbf{u}, \mathbf{v} + \mathbf{w} \rangle = \langle \mathbf{L}, \mathbf{x}, \mathbf{z}, \mathbf{v} \rangle + \langle \mathbf{L}, \mathbf{x}, \mathbf{z}, \mathbf{w} \rangle + \langle \mathbf{L}, \mathbf{x}, \mathbf{u}, \mathbf{v} \rangle + \langle \mathbf{L}, \mathbf{x}, \mathbf{u}, \mathbf{w} \rangle$$

$$+ \langle \mathbf{L}, \mathbf{y}, \mathbf{z}, \mathbf{v} \rangle + \langle \mathbf{L}, \mathbf{y}, \mathbf{z}, \mathbf{w} \rangle + \langle \mathbf{L}, \mathbf{y}, \mathbf{u}, \mathbf{v} \rangle + \langle \mathbf{L}, \mathbf{y}, \mathbf{u}, \mathbf{w} \rangle,$$

$$\langle \mathbf{L}, \mathbf{U}\mathbf{x}, \mathbf{V}\mathbf{y}, \mathbf{W}\mathbf{z} \rangle = \langle\langle \mathbf{L}, \mathbf{U}, \mathbf{V}, \mathbf{W} \rangle, \mathbf{x}, \mathbf{y}, \mathbf{z} \rangle,$$

$$\mathbf{U}\langle \mathbf{L}, \mathbf{x}, \mathbf{y}, \mathbf{z} \rangle = \langle \mathbf{U}\mathbf{L}, \mathbf{x}, \mathbf{y}, \mathbf{z} \rangle,$$

where $\mathbf{U}$, $\mathbf{V}$, and $\mathbf{W}$ are second-order matrices, $\mathbf{K}$ and $\mathbf{S}$ are third-order matrices, and $\mathbf{L}$ is a fourth-order matrix. The corresponding operations with matrices are defined as

$$\langle \mathbf{K}, \mathbf{U}, \mathbf{V} \rangle := \left[K_{jlm}U_{lq}V_{ms}\right], \quad \langle \mathbf{K}, \mathbf{U}, \mathbf{S} \rangle := \left[K_{jlm}U_{lq}S_{mst}\right],$$
$$\langle \mathbf{K}, \mathbf{S}, \mathbf{U} \rangle := \left[K_{jlm}S_{lqs}U_{mt}\right], \quad \langle \mathbf{L}, \mathbf{U}, \mathbf{V}, \mathbf{W} \rangle := \left[L_{jlmq}U_{ls}V_{mt}W_{qx}\right]. \tag{19}$$

This means that multiplications denoted by angle brackets are carried out with respect to the last indices of the first operand and the first index of the other operands. These notations will be exploited along this section.

Now, we derive the coefficient matrices $\mathbf{A}$, $\mathbf{B}$, and $\mathbf{C}$ in Equation (15) from map (12). Similarly to Equation (15), map (12) can be represented in the form

$$\mathbf{z}_{k+1} = \mathbf{J}_k\mathbf{z}_k + \frac{1}{2}\langle \mathbf{K}_k, \mathbf{z}_k, \mathbf{z}_k \rangle + \frac{1}{6}\langle \mathbf{L}_k, \mathbf{z}_k, \mathbf{z}_k, \mathbf{z}_k \rangle + \mathcal{O}\left(\|\mathbf{z}_k\|^4\right). \tag{20}$$

Matrices $\mathbf{K}_k$, and $\mathbf{L}_k$ are defined by

$$\mathbf{K} = \left[K_{jlm}\right] = \left[\partial_l \partial_m H_j\big|_0\right], \quad \mathbf{L} = \left[L_{jlmq}\right] = \left[\partial_l \partial_m \partial_q H_j\big|_0\right], \tag{21}$$

where the semidiscretization index k was dropped in order to avoid confusion with the indices of the matrices. Let us derive $\mathbf{z}_1, \mathbf{z}_2, \ldots, \mathbf{z}_p$ as a function of $\mathbf{z}_0$ using map (20) successively, while dropping all the terms of $\mathcal{O}(\|\mathbf{z}_0\|^4)$ at each step. For $k = 0$, we get

$$\mathbf{z}_1 = \mathbf{J}_0\mathbf{z}_0 + \frac{1}{2}\langle \mathbf{K}_0, \mathbf{z}_0, \mathbf{z}_0 \rangle + \frac{1}{6}\langle \mathbf{L}_0, \mathbf{z}_0, \mathbf{z}_0, \mathbf{z}_0 \rangle + \mathcal{O}\left(\|\mathbf{z}_0\|^4\right), \tag{22}$$

where $\mathbf{z}_1$ is already expressed using $\mathbf{z}_0$. For $k = 1$, we obtain

$$\mathbf{z}_2 = \mathbf{J}_1\mathbf{z}_1 + \frac{1}{2}\langle\mathbf{K}_1, \mathbf{z}_1, \mathbf{z}_1\rangle + \frac{1}{6}\langle\mathbf{L}_1, \mathbf{z}_1, \mathbf{z}_1, \mathbf{z}_1\rangle + \mathcal{O}\left(\|\mathbf{z}_1\|^4\right), \tag{23}$$

where $\mathbf{z}_1$ should be substituted from Equation (22) in order to get $\mathbf{z}_2$ as a function of $\mathbf{z}_0$. When substituting Equation (22), we drop the terms of $\mathcal{O}(\|\mathbf{z}_0\|^4)$ and use the properties (18), by which we obtain

$$\mathbf{z}_2 = \mathbf{J}_1\mathbf{J}_0\mathbf{z}_0 + \frac{1}{2}\mathbf{J}_1\langle\mathbf{K}_0, \mathbf{z}_0, \mathbf{z}_0\rangle + \frac{1}{6}\mathbf{J}_1\langle\mathbf{L}_0, \mathbf{z}_0, \mathbf{z}_0, \mathbf{z}_0\rangle + \frac{1}{2}\langle\langle\mathbf{K}_1, \mathbf{J}_0, \mathbf{J}_0\rangle, \mathbf{z}_0, \mathbf{z}_0\rangle + \frac{1}{4}\langle\langle\mathbf{K}_1, \mathbf{J}_0, \mathbf{K}_0\rangle, \mathbf{z}_0, \mathbf{z}_0, \mathbf{z}_0\rangle$$
$$+ \frac{1}{4}\langle\langle\mathbf{K}_1, \mathbf{K}_0, \mathbf{J}_0\rangle, \mathbf{z}_0, \mathbf{z}_0, \mathbf{z}_0\rangle + \frac{1}{6}\langle\langle\mathbf{L}_1, \mathbf{J}_0, \mathbf{J}_0, \mathbf{J}_0\rangle, \mathbf{z}_0, \mathbf{z}_0, \mathbf{z}_0\rangle + \mathcal{O}\left(\|\mathbf{z}_0\|^4\right). \tag{24}$$

In a similar manner, we can obtain $\mathbf{z}_3, \mathbf{z}_4, \ldots, \mathbf{z}_p$ by recursively using Equation (20). The final form of $\mathbf{z}_p$ becomes

$$\mathbf{z}_p = \mathbf{A}\mathbf{z}_0 + \frac{1}{2}\langle\tilde{\mathbf{B}}, \mathbf{z}_0, \mathbf{z}_0\rangle + \frac{1}{6}\langle\tilde{\mathbf{C}}, \mathbf{z}_0, \mathbf{z}_0, \mathbf{z}_0\rangle + \mathcal{O}\left(\|\mathbf{z}_0\|^4\right), \tag{25}$$

where the coefficient matrices are

$$\mathbf{A} = \mathbf{Q}_{p-1,0},$$
$$\tilde{\mathbf{B}} = \sum_{j=0}^{p-1}\mathbf{Q}_{p-1,j+1}\langle\mathbf{K}_j, \mathbf{Q}_{j-1,0}, \mathbf{Q}_{j-1,0}\rangle,$$
$$\tilde{\mathbf{C}} = \sum_{j=0}^{p-1}\mathbf{Q}_{p-1,j+1}\langle\mathbf{L}_j, \mathbf{Q}_{j-1,0}, \mathbf{Q}_{j-1,0}, \mathbf{Q}_{j-1,0}\rangle + \frac{3}{2}\sum_{j=1}^{p-1}\mathbf{Q}_{p-1,j+1}\left\langle\mathbf{K}_j, \mathbf{Q}_{j-1,0}, \sum_{l=0}^{j-1}\mathbf{Q}_{j-1,l+1}\langle\mathbf{K}_l, \mathbf{Q}_{l-1,0}, \mathbf{Q}_{l-1,0}\rangle\right\rangle \tag{26}$$
$$+ \frac{3}{2}\sum_{j=1}^{p-1}\mathbf{Q}_{p-1,j+1}\left\langle\mathbf{K}_j, \sum_{l=0}^{j-1}\mathbf{Q}_{j-1,l+1}\langle\mathbf{K}_l, \mathbf{Q}_{l-1,0}, \mathbf{Q}_{l-1,0}\rangle, \mathbf{Q}_{j-1,0}\right\rangle$$

with the following notations

$$\mathbf{Q}_{j,j+1} := \mathbf{I}, \quad \mathbf{Q}_{j,l} := \mathbf{J}_j\mathbf{J}_{j-1}\cdots\mathbf{J}_{l+1}\mathbf{J}_l, \quad l \leq j, \quad j = 0, \ldots, p-1. \tag{27}$$

Note that $\mathbf{Q}_{j,l}$ represents the linear dynamics from the lth to the $(j+1)$st time instant, that is, $\mathbf{Q}_{j-1,0}$ describes the linear dynamics from the 0th to the jth time instant, whereas $\mathbf{Q}_{p-1,j+1}$ represents the linear dynamics from the $(j+1)$st to the pth time instant. Thus, the terms in $\tilde{\mathbf{B}}$ in Equation (26) can be interpreted such that the linear dynamics governs up to the jth time instant ($\mathbf{Q}_{j-1,0}$), where the quadratic term has its effect ($\mathbf{K}_j$), and then the linear dynamics operates again from the $(j+1)$st instant ($\mathbf{Q}_{p-1,j+1}$), and the results for all possible values of j are added. The cubic term with $\tilde{\mathbf{C}}$ is similarly constructed from the effect of 2 quadratic terms ($\mathbf{K}_j$ and $\mathbf{K}_l$) or a single cubic term ($\mathbf{L}_j$) and linear maps at all other time instants. Since we do not use the terms of $\mathcal{O}(\|\mathbf{z}_0\|^4)$, no other combination of nonlinear terms needs to be considered.

Finally, note that matrices $\mathbf{B}$ and $\mathbf{C}$ in Equations (15) and (16) and $\tilde{\mathbf{B}}$ and $\tilde{\mathbf{C}}$ in Equations (25) and (26) are not necessarily the same; the coefficient matrices of the nonlinear terms are nonunique as different $\mathbf{B}$ and $\mathbf{C}$ matrices can produce the same expressions for $\langle\mathbf{B}, \mathbf{z}_0, \mathbf{z}_0\rangle$ and $\langle\mathbf{C}, \mathbf{z}_0, \mathbf{z}_0, \mathbf{z}_0\rangle$, respectively. However, the matrices $\mathbf{B}$ and $\mathbf{C}$ given by Equation (16) originate in second and third derivatives; thus, they are symmetric to their last two and three indices, respectively: $B_{jlm} = B_{jml}$ and $C_{jlmq} = C_{jlqm} = C_{jmlq} = C_{jmql} = C_{jqlm} = C_{jqml}$. Therefore, it can be shown that $\mathbf{B}$ and $\mathbf{C}$ in Equation (16) are the symmetric parts of $\tilde{\mathbf{B}}$ and $\tilde{\mathbf{C}}$ in Equation (26), respectively, which implies

$$\mathbf{B} = \text{sym}(\tilde{\mathbf{B}}) = \frac{1}{2}\left[\tilde{B}_{jlm} + \tilde{B}_{jml}\right],$$
$$\mathbf{C} = \text{sym}(\tilde{\mathbf{C}}) = \frac{1}{6}\left[\tilde{C}_{jlmq} + \tilde{C}_{jlqm} + \tilde{C}_{jmlq} + \tilde{C}_{jmql} + \tilde{C}_{jqlm} + \tilde{C}_{jqml}\right]. \tag{28}$$

Notice that according to Equation (26), matrix $\tilde{\mathbf{B}}$ is in fact symmetric and $\mathbf{B} = \tilde{\mathbf{B}}$, whereas $\tilde{\mathbf{C}}$ is not symmetric and $\mathbf{C} \neq \tilde{\mathbf{C}}$.

4 | BIFURCATION ANALYSIS

In this section, we perform bifurcation analysis based on map (15). In order to emphasize that this map describes the evolution over the principal period of length $T = p\Delta t$ (ie, over p semidiscretization steps), we introduce a new index

$K \in \mathbb{N}$ that denotes the number of principal periods elapsed. Introducing $\mathbf{Z}_K = \mathbf{z}_{Kp}$, map (15) can be rewritten as

$$\mathbf{Z}_{K+1} = \mathbf{A}\mathbf{Z}_K + \frac{1}{2}\langle \mathbf{B}, \mathbf{Z}_K, \mathbf{Z}_K \rangle + \frac{1}{6}\langle \mathbf{C}, \mathbf{Z}_K, \mathbf{Z}_K, \mathbf{Z}_K \rangle + \mathcal{O}\left(\|\mathbf{Z}_K\|^4\right). \tag{29}$$

Once the coefficient matrices $\mathbf{A}$, $\mathbf{B}$, and $\mathbf{C}$ are calculated from Equations (26)-(28), map (29) can be used for bifurcation analysis. The bifurcation theory of nonlinear maps is discussed in the work of Kuznetsov[20]; from this point on, we apply the formulas presented therein. Note that Neimark-Sacker, flip, and fold bifurcations of the fixed point $\mathbf{Z} = \mathbf{0}$ of map (29) correspond to secondary Hopf (torus), period doubling, and cyclic fold bifurcations of the periodic orbit $\mathbf{y}_p(t)$ of Equation (1). Here, we demonstrate the analysis of Neimark-Sacker bifurcation in detail, and we address the differences for flip and fold bifurcations.

4.1 | Neimark-Sacker bifurcation

Let $\alpha \in \mathbb{R}$ denote the bifurcation parameter, and let α_{cr} be the Neimark-Sacker bifurcation point. The bifurcation of the fixed point is determined by the eigenvalues of the coefficient matrix $\mathbf{A}$, which are given by the characteristic equation $\det(\mu\mathbf{I} - \mathbf{A}) = 0$. At Neimark-Sacker bifurcation, a pair of complex conjugate eigenvalues is located on the unit circle of the complex plane, that is, there exists a critical eigenvalue

$$\mu_{cr} = e^{i\theta_0}, \quad |\mu|_{cr} = 1, \tag{30}$$

where $i^2 = -1$, $\theta_0 \in (0, \pi)$. From this point on, subscript cr refers to the substitution $\mu = \mu_{cr}$, $\alpha = \alpha_{cr}$. We can determine the left and right eigenvectors $\mathbf{p}$ and $\mathbf{q}$ of the linear coefficient matrix $\mathbf{A}_{cr}$ associated with the critical eigenvalue μ_{cr} by solving

$$\mathbf{A}_{cr}\mathbf{q} = \mu_{cr}\mathbf{q}, \quad \mathbf{p}\mathbf{A}_{cr} = \overline{\mu}_{cr}\mathbf{p}, \quad \overline{\mathbf{p}}\mathbf{q} = 1, \tag{31}$$

where the overbar indicates complex conjugate.

The analysis of the Neimark-Sacker bifurcation can be done via center manifold reduction.[20] Accordingly, the dynamics of map (29) is restricted to a 2-dimensional (2D) center manifold spanned by (the real and imaginary parts of) $\mathbf{q}$ and $\overline{\mathbf{q}}$. The approximation of the 2D restricted map can be written in polar form as

$$\begin{aligned}
\hat{\rho}_{K+1} &= \hat{\rho}_K + |\mu|'_{cr}(\alpha - \alpha_{cr})\hat{\rho}_K + a_{cr}\hat{\rho}_K^3 + \mathcal{O}\left(\hat{\rho}_K^4\right), \\
\hat{\theta}_{K+1} &= \hat{\theta}_K + \theta_0 + \mathcal{O}\left(\hat{\rho}_K^2\right),
\end{aligned} \tag{32}$$

where $\hat{\rho}$ is the amplitude and $\hat{\theta}$ is the phase angle. Note that the coefficients of $\hat{\rho}_K$, $\hat{\rho}_K^3$, and $\hat{\theta}_K^0 = 1$ are approximated by linear and constant functions of the bifurcation parameter α; this approximation is valid only in the vicinity of the bifurcation ($\alpha \approx \alpha_{cr}$). The prime indicates a derivative with respect to the bifurcation parameter α, $|\mu|'_{cr}$ is the root tendency (the radial speed by which the critical eigenvalues cross the unit circle), and a_{cr} is the leading coefficient for which a closed-form formula is available in the work of Kuznetsov[20] (see below).

In Equation (32), the map for the amplitude $\hat{\rho}$ has a nontrivial fixed point

$$\rho = \sqrt{-\frac{|\mu|'_{cr}(\alpha - \alpha_{cr})}{a_{cr}}} + \mathcal{O}(\alpha). \tag{33}$$

On the 2D center manifold, this nontrivial fixed point corresponds to a critical solution that is located on an isolated closed invariant curve with radius ρ. The genericity conditions related to the existence and uniqueness of the closed invariant curve are the transversality condition $|\mu|'_{cr} \neq 0$ and the nondegeneracy conditions $\mu_{cr}^m \neq 1$, $m = 1, 2, 3, 4$, $a_{cr} \neq 0$ (see the work of Kuznetsov[20]). Here, we assume that these conditions are satisfied. The critical solution associated with the closed invariant curve is

$$\mathbf{Z}_K = \rho e^{iK\theta_0}\mathbf{q} + \rho e^{-iK\theta_0}\overline{\mathbf{q}}. \tag{34}$$

In order to obtain solution (34), the root tendency $|\mu|'_{cr}$ and the leading coefficient a_{cr} must be determined. The calculation of the root tendency $|\mu|'_{cr}$ can be reduced to determining the constant μ'_{cr} and using the relationship[22]

$$|\mu|' = \frac{1}{|\mu|}\mathrm{Re}\left(\overline{\mu}\mu'\right) \tag{35}$$

for the critical case $\mu = \mu_{cr}$. The constant μ'_{cr} can be obtained by the implicit differentiation of the characteristic equation $\det(\mu\mathbf{I} - \mathbf{A}) = 0$:

$$\mu'_{cr} = \left.\frac{d\mu}{d\alpha}\right|_{cr} = -\left.\frac{\frac{\partial}{\partial\alpha}\det(\mu\mathbf{I} - \mathbf{A})}{\frac{\partial}{\partial\mu}\det(\mu\mathbf{I} - \mathbf{A})}\right|_{cr} = -\frac{\mathrm{tr}(\mathrm{adj}(\mu_{cr}\mathbf{I} - \mathbf{A}_{cr})(-\mathbf{A}'_{cr}))}{\mathrm{tr}(\mathrm{adj}(\mu_{cr}\mathbf{I} - \mathbf{A}_{cr}))}. \tag{36}$$

Note that derivative $\mathbf{A}'$ can be given using the derivative $\mathbf{J}'_j$ of the linear coefficient matrices of each semi-discretization step:

$$\mathbf{A}' = \sum_{j=0}^{p-1} \mathbf{Q}_{p-1,j+1} \mathbf{J}'_j \mathbf{Q}_{j-1,0}. \tag{37}$$

As for the leading coefficient a_{cr}, formula (5.74) in the work of Kuznetsov[20] can directly be used:

$$a_{cr} = \frac{1}{2}\mathrm{Re}\left(e^{-i\theta_0}\left(\overline{\mathbf{p}}\langle\mathbf{C}_{cr},\mathbf{q},\mathbf{q},\overline{\mathbf{q}}\rangle + 2\overline{\mathbf{p}}\langle\mathbf{B}_{cr},\mathbf{q},(\mathbf{I} - \mathbf{A}_{cr})^{-1}\langle\mathbf{B}_{cr},\mathbf{q},\overline{\mathbf{q}}\rangle\rangle + \overline{\mathbf{p}}\langle\mathbf{B}_{cr},\overline{\mathbf{q}},\left(e^{2i\theta_0}\mathbf{I} - \mathbf{A}_{cr}\right)^{-1}\langle\mathbf{B}_{cr},\mathbf{q},\mathbf{q}\rangle\rangle\right)\right). \tag{38}$$

Notice that the magnitude (norm) of the eigenvector $\mathbf{q}$ is not determined by Equation (31); it can be chosen arbitrarily. When multiplying the eigenvector $\mathbf{q}$ by a constant $c \in \mathbb{C}$, the coefficient a_{cr} scales by $|c|^2$, the amplitude ρ scales by $1/|c|$, while the critical solution (34) remains the same. Also note that if the lth component of $\mathbf{q}$ is selected to be $q_l = 1/2$, then ρ represents the amplitude of the lth component of solution (34) as $Z_{K,l} = \rho\cos(K\theta_0)$. Otherwise, Equation (34) implies $Z_{K,l} = 2|q_l|\rho\cos(K\theta_0 + \vartheta_l)$, where ϑ_l is a certain phase shift and $2|q_l|\rho$ represents the amplitude of the lth component of solution (34).

The critical solution (34) corresponds to a quasi-periodic solution $\mathbf{y}_{qp}(t)$ of flow (1) that may simplify to a periodic solution in special cases. The stability of the quasi-periodic solution is the same as the stability of the closed invariant curve associated with Neimark-Sacker bifurcation, which is determined by the sign of the leading coefficient a_{cr}. If $a_{cr} < 0$, the Neimark-Sacker bifurcation is supercritical and solution (34) is stable, whereas if $a_{cr} > 0$, the bifurcation is subcritical and the solution is unstable.

In addition, the fixed point ρ is related to the amplitude of the quasi-periodic solution $\mathbf{y}_{qp}(t)$. Suppose that we are interested in the half r of the peak-to-peak amplitude in terms of the jth coordinate $y_{qp,j}(t)$ of the vector $\mathbf{y}_{qp}(t)$. Then, the amplitude r_p of the periodic solution $y_{p,j}(t)$ must be added to the amplitude r_u of the perturbation $u_j(t)$ that can be determined from ρ as follows. According to Equation (13), the jth, $(j + n)$th, ..., $(j + rn)$th elements of solution (34) are $u_{Kp,j}, u_{Kp-1,j}, \ldots, u_{Kp-r,j}$. These discrete-time solutions vary with amplitudes $\rho_0, \rho_1, \ldots, \rho_r$, where the largest of them approximates the amplitude of $u_j(t)$: $r_u = \max(\rho_m), m = 1, 2, \ldots, r$. The amplitudes ρ_m can be obtained from Equation (33) provided that the eigenvector $\mathbf{q}$ is chosen such that $q_{j+mn} = 1/2$. Equivalently, instead of determining $\rho_0, \rho_1, \ldots, \rho_r$, we can calculate the leading coefficient a_{cr} from Equation (38) using an eigenvector $\mathbf{q}$ with arbitrary norm, and then scale it as

$$\tilde{a}_{cr} = \frac{a_{cr}}{4\max_{0\leq m\leq r}\left(|q_{j+mn}|^2\right)}. \tag{39}$$

This way, Equation (33) gives r_u directly:

$$r_u = \sqrt{-\frac{|\mu|'_{cr}(\alpha - \alpha_{cr})}{\tilde{a}_{cr}}}. \tag{40}$$

In summary, the amplitude $r = r_p + r_u$ and the stability of the quasi-periodic solution can be determined by Equations (35)-(40), where the formulas of the coefficient matrices $\mathbf{A}_{cr}$, $\mathbf{B}_{cr}$, and $\mathbf{C}_{cr}$ are given by Equations (26)-(28).

4.2 | Flip bifurcation

The analysis of flip bifurcation is similar to that presented for Neimark-Sacker bifurcation. At flip bifurcation, the critical eigenvalue $\mu_{cr} = -1$ is located on the unit circle of the complex plane. The corresponding eigenvectors $\mathbf{p}$ and $\mathbf{q}$ are real, and $\mathbf{q}$ spans a 1-dimensional center manifold. The restriction of map (29) to this manifold has the equivalent form

$$\hat{\rho}_{K+1} = -\hat{\rho}_K - \mu'_{cr}(\alpha - \alpha_{cr})\hat{\rho}_K - a_{cr}\hat{\rho}_K^3 + \mathcal{O}\left(\hat{\rho}_K^4\right) \tag{41}$$

provided that the transversality condition $\mu'_{cr} \neq 0$ and the nondegeneracy condition $a_{cr} \neq 0$ are fulfilled.[20]
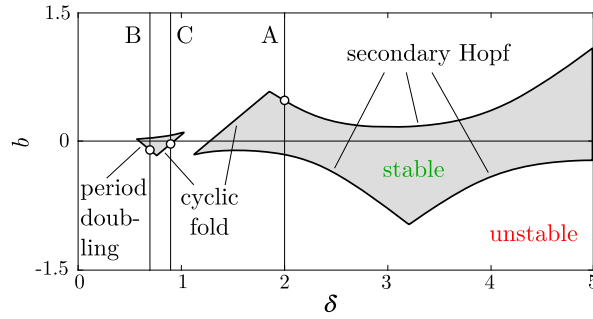
FIGURE 1 Stability chart of the delayed Mathieu-Duffing equation (49) for $a_1 = 0.1$, $\varepsilon = 1$, and $\tau = 2\pi$. Vertical lines at $\delta = 2, 0.7$, and 0.9 correspond to the bifurcation diagrams shown in Figures 2, 3, and 4, respectively [Colour figure can be viewed at wileyonlinelibrary.com]

The second iterate of map (41) has a nontrivial fixed point ρ given by Equation (33). This fixed point corresponds to a period-2 solution of map (29) that approximately reads

$$\mathbf{Z}_K = \rho(-1)^K \mathbf{q} \tag{42}$$

and is associated with a period-2 solution of flow (1). The stability of the period-2 solution is determined by the sign of a_{cr} (it is stable for $a_{\text{cr}} < 0$ and unstable for $a_{\text{cr}} > 0$), whereas its approximate amplitude $r = r_{\text{p}} + r_u$ can be obtained the same way as that of the quasi-periodic orbit in the previous section. That is, the constant μ'_{cr} is real ($|\mu|'_{\text{cr}} = \mu'_{\text{cr}}$) and can be calculated according to Equation (36). Meanwhile, the expression of the leading coefficient modifies to

$$a_{\text{cr}} = -\frac{1}{6}\mathbf{p}\langle \mathbf{C}_{\text{cr}}, \mathbf{q}, \mathbf{q}, \mathbf{q} \rangle + \frac{1}{2}\mathbf{p}\left\langle \mathbf{B}_{\text{cr}}, \mathbf{q}, (\mathbf{A}_{\text{cr}} - \mathbf{I})^{-1}\langle \mathbf{B}_{\text{cr}}, \mathbf{q}, \mathbf{q} \rangle \right\rangle; \tag{43}$$

see the formulas after equation (5.69) in the work of Kuznetsov.[20] The following scaled coefficient can be used to obtain the amplitude of the period-2 solution from Equation (40):

$$\tilde{a}_{\text{cr}} = \frac{a_{\text{cr}}}{\max\limits_{0 \leq m \leq r} \left(q_{j+mn}^2 \right)}. \tag{44}$$

4.3 | Fold bifurcation

In the case of fold bifurcation, the critical eigenvalue is $\mu_{\text{cr}} = 1$, the eigenvectors $\mathbf{p}$ and $\mathbf{q}$ are real, and $\mathbf{q}$ spans a 1-dimensional center manifold. Restriction to this manifold yields the critical system[20]

$$\hat{\rho}_{K+1} = \hat{\rho}_K + \mu'_{\text{cr}}(\alpha - \alpha_{\text{cr}})\hat{\rho}_K + \sigma_{\text{cr}}\hat{\rho}_K^2 + a_{\text{cr}}\hat{\rho}_K^3 + \mathcal{O}\left(\hat{\rho}_K^4 \right). \tag{45}$$

According to the formulas after equation (5.68) in the work of Kuznetsov,[20] the critical normal form coefficients read

$$\sigma_{\text{cr}} = \frac{1}{2}\mathbf{p}\langle \mathbf{B}_{\text{cr}}, \mathbf{q}, \mathbf{q} \rangle, \tag{46}$$

$$a_{\text{cr}} = \frac{1}{6}\mathbf{p}\langle \mathbf{C}_{\text{cr}}, \mathbf{q}, \mathbf{q}, \mathbf{q} \rangle - \frac{1}{2}\mathbf{p}\left\langle \mathbf{B}_{\text{cr}}, \mathbf{q}, (\mathbf{A}_{\text{cr}} - \mathbf{I})^{\text{INV}}\mathbf{d} \right\rangle, $$
$$\mathbf{d} = \langle \mathbf{B}_{\text{cr}}, \mathbf{q}, \mathbf{q} \rangle - (\mathbf{p}\langle \mathbf{B}_{\text{cr}}, \mathbf{q}, \mathbf{q} \rangle)\mathbf{q}, \tag{47}$$

where $(\mathbf{A}_{\text{cr}} - \mathbf{I})^{\text{INV}}\mathbf{d}$ is obtained by solving the following equation for $\mathbf{w}$:

$$\begin{bmatrix} \mathbf{A}_{\text{cr}} - \mathbf{I} & \mathbf{q} \\ \mathbf{p} & 0 \end{bmatrix} \begin{bmatrix} \mathbf{w} \\ v \end{bmatrix} = \begin{bmatrix} \mathbf{d} \\ 0 \end{bmatrix}. \tag{48}$$

Note that since $\mu_{\text{cr}} = 1$ is an eigenvalue of $\mathbf{A}_{\text{cr}}$, the matrix $\mathbf{A}_{\text{cr}} - \mathbf{I}$ is singular. Thus, its inverse does not exist, and instead, we use $(\mathbf{A}_{\text{cr}} - \mathbf{I})^{\text{INV}}$ as defined above. The nondegeneracy condition associated with cyclic fold bifurcation is $\sigma_{\text{cr}} \neq 0$.[20]

5 | A CASE STUDY: THE DELAYED MATHIEU-DUFFING EQUATION

In this section, we demonstrate the bifurcation analysis via semidiscretization for the delayed Mathieu-Duffing equation:

$$\ddot{x}(t) + a_1\dot{x}(t) + (\delta + \varepsilon \cos t)x(t) + \mu x^3(t) = bx(t - \tau). \tag{49}$$
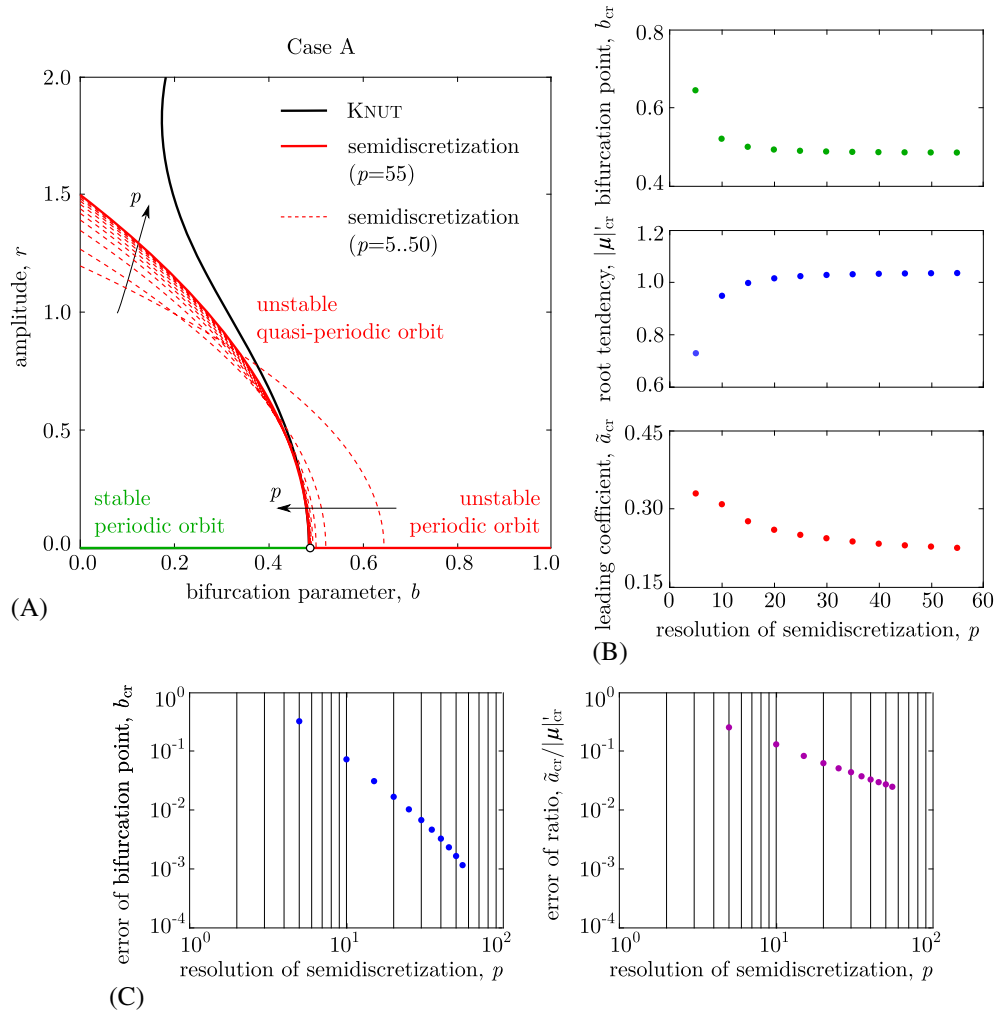
FIGURE 2 A, Bifurcation diagrams of the delayed Mathieu-Duffing equation near a secondary Hopf bifurcation assuming case A of Figure 1 with $\mu = 0.5$ and $\delta = 2$; B, The convergence of the normal form coefficients; C, The error relative to the solution of KNUT [Colour figure can be viewed at wileyonlinelibrary.com]

This equation was analyzed by the method of averaging in the work of Morrison and Rand[23] for the undamped case ($a_1 = 0$). Analyses of the Mathieu equation in the absence of delay ($b = 0$) can be found in the works of Ng and Rand[24,25] and Zounes and Rand[26] considering cubic nonlinearities and in the work of Ramani et al[27] for the case of quadratic damping. Other analytical approaches for studying nonlinear delay-free time-periodic systems can also be found in the works of Pandiyan and Sinha,[28] Butcher and Sinha,[29,30] and Sinha et al.[31] The closed-form stability condition and the stability diagram of the linear delayed Mathieu equation ($\mu = 0$) was given in the work of Insperger and Stépán.[32]

Equation (49) defines a nonlinear time-periodic time-delay system that can be represented in the form of Equation (1). We analyze the stability and bifurcations of its periodic solution, ie, the trivial solution $x_p(t) \equiv 0$ itself. We decompose the solution of Equation (49) into the sum of the periodic solution and a perturbation $x(t) = x_p(t) + \xi(t)$ that yields Equation (2) with

$$\mathbf{u}(t) = \begin{bmatrix} \xi(t) \\ \dot{\xi}(t) \end{bmatrix}, \quad \mathbf{D}(t) = \begin{bmatrix} 0 & 1 \\ -(\delta + \varepsilon \cos t) & -a_1 \end{bmatrix}, \quad \mathbf{E}(t) \equiv \mathbf{E} = \begin{bmatrix} 0 & 0 \\ b & 0 \end{bmatrix},$$

$$\mathbf{g}(t, \mathbf{u}(t), \mathbf{u}(t - \tau)) \equiv \mathbf{g}(\mathbf{u}(t)) = \begin{bmatrix} 0 \\ -\mu \xi^3(t) \end{bmatrix}.$$
(50)

Its semidiscretized counterpart is given by Equation (5) with

$$\mathbf{D}_k = \begin{bmatrix} 0 & 1 \\ -\left(\delta + \varepsilon \dfrac{\sin t_{k+1} - \sin t_k}{\Delta t}\right) & -a_1 \end{bmatrix}, \quad \mathbf{g}_k(\mathbf{u}_k) = \begin{bmatrix} 0 \\ -\mu x_k^3 \end{bmatrix}$$
(51)

that can be written in form (12) using Equations (7), (11), and (13).

From this point on, the bifurcation analysis can be carried out according to Section 4. The results are presented in Figures 1-4 for $a_1 = 0.1$, $\varepsilon = 1$, $\mu = 0.5$, and $\tau = 2\pi$. Figure 1 presents the stability chart of the system in the plane (δ, b) that was computed by the semidiscretization method using period resolution $p = 50$. The parameter regions associated with the linearly stable trivial solution are shown by gray shading, whereas the loci of cyclic fold, period doubling, and secondary Hopf bifurcations are also indicated. As shown by the vertical lines B, C, and A in Figure 1, $\delta = 0.7$, $\delta = 0.9$, and $\delta = 2$ are selected for analyzing period doubling, cyclic fold, and secondary Hopf bifurcations, respectively, and b is chosen as a bifurcation parameter. The bifurcation points under analysis are indicated by circles, whereas the corresponding bifurcation diagrams are shown in Figures 2, 3, and 4. The Mathematica code generating these Figures is given in the Appendix.

For $\delta = 2$, a secondary Hopf bifurcation occurs at $b = b_{cr} \approx 0.5$ that gives rise to a quasi-periodic solution. The amplitude r of this solution as a function of the bifurcation parameter b is indicated by red lines in Figure 2A, where semidiscretization with period resolutions $p = 5, 10, \ldots, 50, 55$ was used to obtain the bifurcation diagrams. The results were verified by numerical continuation: thick black line shows the amplitude $\|x(t)\|_\infty$ obtained by the continuation package KNUT.[7,8] The bifurcation point (determined by the value of b_{cr}) and the initial curvature (given by the ratio of $\tilde{a}_{cr}$ and $|\mu|'_{cr}$) of the bifurcation diagrams obtained by semidiscretization converge to those obtained by KNUT. Note, however, that the analysis based on normal forms is valid only in the vicinity of the bifurcation: it cannot catch phenomena such as the fold of the quasi-periodic orbit shown by the thick black line. Figure 2C shows the error of semidiscretization with
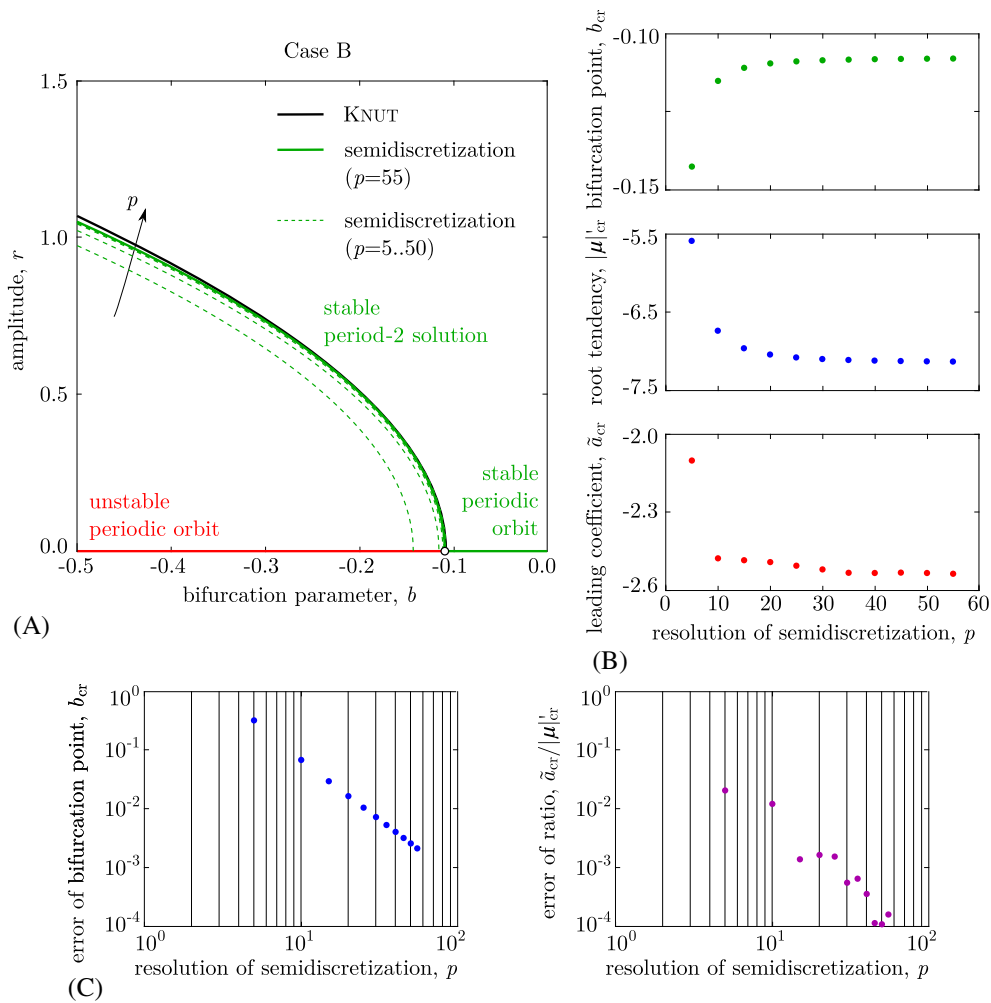

FIGURE 3 A, Bifurcation diagrams of the delayed Mathieu-Duffing equation near a period doubling bifurcation assuming case B of Figure 1 with $\mu = 0.5$ and $\delta = 0.7$; B, The convergence of the normal form coefficients; C, The error relative to the solution of KNUT [Colour figure can be viewed at wileyonlinelibrary.com]
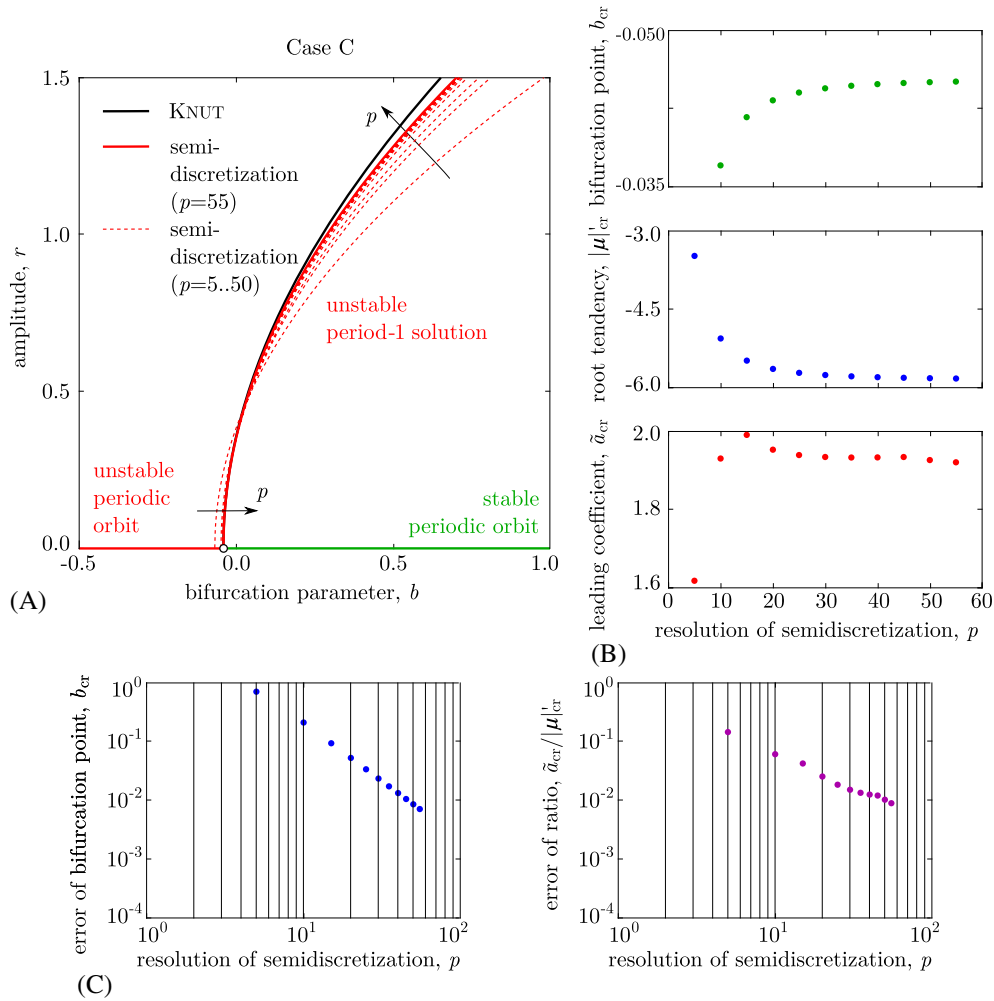
FIGURE 4 A, Bifurcation diagrams of the delayed Mathieu-Duffing equation near a cyclic fold bifurcation assuming case C of Figure 1 with $\mu = 0.5$ and $\delta = 0.9$; B, The convergence of the normal form coefficients; C, The error relative to the solution of KNUT [Colour figure can be viewed at wileyonlinelibrary.com]

different period resolutions relative to the results of KNUT. Notice that KNUT computes a branch of bifurcating solutions, while it does not provide the normal form coefficients directly and only the values of b_{cr} and $\tilde{a}_{cr}/|\mu|'_{cr}$ are determined by the branch. Therefore, we used the first point of the branch as bifurcation point b_{cr}, and we calculated the ratio $\tilde{a}_{cr}/|\mu|'_{cr}$ from the initial curvature of the branch via fitting a parabola to its first 25 points and using Equation (40). According to the Figure, the approach of KNUT and the method of this paper converge to the same result. The convergence of semidiscretization is also illustrated in Figure 2B, where the values of b_{cr}, $|\mu|'_{cr}$, and $\tilde{a}_{cr}$ are shown as a function of the period resolution p. Note that the sign of $\tilde{a}_{cr}$ that determines the stability of the arising quasi-periodic orbit is correct even for the smallest value of p. This implies that even a rough discretization is sufficient to determine the sense (criticality) of a bifurcation.

Figure 3 shows the bifurcation diagrams and the normal form coefficients of a period doubling bifurcation occurring for $\delta = 0.7$. The bifurcation gives rise to a stable period-2 branch that is shown by green lines for semidiscretization with period resolutions $p = 5, 10, \ldots, 50, 55$. The thick black line shows the result of numerical continuation using KNUT. In this case, the bifurcation diagrams obtained by the two methods almost overlap, and the approximate amplitude obtained by normal form analysis is valid for the depicted range of the bifurcation parameter. In addition, the sign of the leading coefficient $\tilde{a}_{cr}$ is again the same for all values of p; thus, even a small period resolution is suitable to analyze the criticality of the bifurcation.

Figure 4 shows the case of a cyclic fold bifurcation for $\delta = 0.9$. Note that the bifurcation is nongeneric in this case, since the normal form coefficient σ_{cr} in Equation (45) is zero as the coefficient $\mathbf{B}$ of the quadratic terms is a zero matrix.
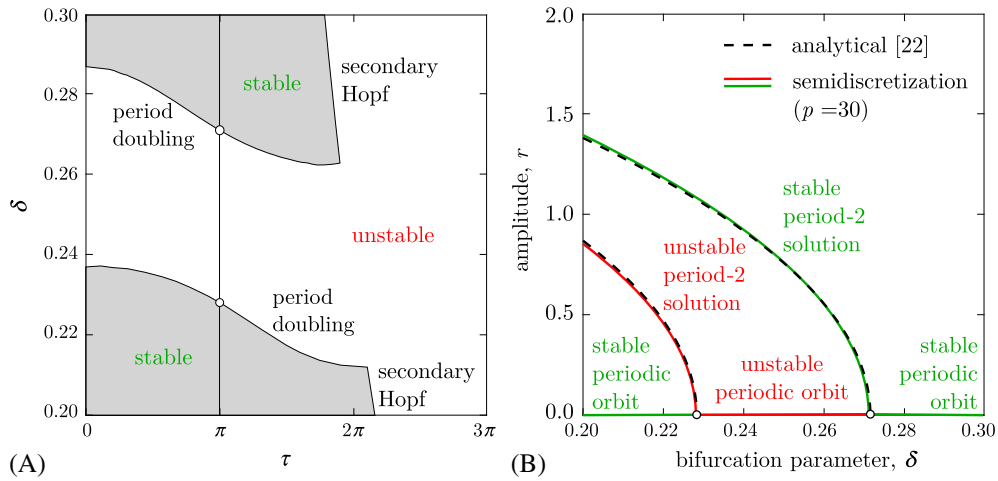
FIGURE 5 A, Stability chart of the delayed Mathieu-Duffing equation (49) for $a_1 = 0$, $\varepsilon = 0.05$, and $b = 0.0125$; B, Bifurcation diagrams assuming $\mu = 0.05$ and $\tau = \pi$ [Colour figure can be viewed at wileyonlinelibrary.com]

The bifurcation associated with map (45) is therefore a pitchfork bifurcation that gives rise to an unstable branch of a nontrivial periodic solution. The amplitude of this solution can be obtained the same way as that of the period-2 orbit associated with period doubling bifurcation, via Equations (40) and (44). The results of semidiscretization (shown by red lines) are again in agreement with those obtained by numerical continuation using KNUT (shown by a thick black line).

Finally, we make a comparison with the results in the work of Morrison and Rand,[23] where the undamped case $a_1 = 0$ was investigated analytically using the method of averaging by assuming small ε, μ, and b values and considering the vicinity of $\delta = 1/4$. We consider example 1 in the work of Morrison and Rand[23] with parameters $\varepsilon = 0.05$, $\mu = 0.05$, and $b = 0.0125$ (these correspond to $\alpha = 1$, $\beta = 0.25$, $\gamma = 1$, and $\varepsilon = 0.05$ using the notations in the aforementioned work[23]). Figure 5A shows the stability chart of the associated linear system in the plane (τ, δ) for $\tau \in [0, 3\pi]$ and $\delta \in [0.2, 0.3]$ (these correspond to $T \in [0, 3\pi]$ and $\delta_1 \in [-1, 1]$ using the notations in the work of Morrison and Rand[23]). Here, the semidiscretization method with period resolution $p = 30$ was used to compute the stability chart; the corresponding figure obtained by averaging is shown in Figure 10 in the aforementioned work.[23] Figure 5B shows the bifurcation diagrams for $\tau = \pi$ that corresponds to the solid vertical line in Figure 5A. For $\tau = \pi$, the trivial solution $x(t) \equiv 0$ undergoes period doubling bifurcations when its stability changes at $\delta \approx 0.23$ and $\delta \approx 0.27$. The bifurcations give rise to period-2 orbits. In the work of Morrison and Rand,[23] the following approximate analytical formula was derived for the amplitude of the arising orbits:

$$r = \sqrt{\frac{4}{3\mu}\left(b\cos\left(\frac{\tau}{2}\right) - \left(\delta - \frac{1}{4}\right) \pm \frac{1}{2}\sqrt{\varepsilon^2 - 4b^2\sin^2\left(\frac{\tau}{2}\right)}\right)}, \tag{52}$$

see Equation (19) in the work of Morrison and Rand.[23] The amplitude r obtained using formula (52) is shown by dashed lines in Figure 5B, and the results of semidiscretization for period resolution $p = 30$ are shown by solid lines. The approximate analytical results obtained by averaging agree well with the numerical results of semidiscretization.

6 | CONCLUSIONS

In this paper, we have presented an approach to analyze bifurcations of periodic solutions associated with time-periodic DDEs. The method uses normal form coefficients to unfold the possible bifurcation scenarios and to determine the amplitude and stability of solutions arising from bifurcation. To this end, we discretized the solution operator of the time-periodic DDE by a sequence of nonlinear maps using the semidiscretization technique. Extension to systems with distributed and time-periodic time delays is also possible via semidiscretization. Note, however, that other discretization schemes that lead to a sequence of nonlinear maps could also be used; the analysis built on these maps would be the

same. The main contribution of this work is the algorithm to combine the subsequent maps to a single resultant map that enables us to analyze bifurcations via the center manifold theory. The analysis of the fixed point reveals the behavior of the periodic solution related to the original time-periodic DDE, as well as the stability and amplitude of the bifurcating orbits.

The computational costs of semidiscretization are determined by the resolution of the time period and the delay. The delay resolution r affects memory consumption and the dimension of eigenproblems to be solved in Equation (31), since the coefficient matrices $\mathbf{A}$, $\mathbf{B}$, and $\mathbf{C}$ are of size $(r + 1)n$. This dimension can be reduced for dynamical systems that do not involve time delays in all state variables, since the corresponding delayed states can be omitted from vector $\mathbf{z}_k$ in Equation (13). This is also the case for the delayed Mathieu-Duffing equation (49), where $\dot{x}$ does not show up with a retarded argument. The period resolution p affects the number of matrix multiplications in Equations (26) and (27), which is $2p^2 + 8p - 10$. In systems where second-order terms are absent (such as in the delayed Mathieu-Duffing equation), the number of matrix multiplications decreases to $(p^2 + 7p - 8)/2$, because the terms containing $\mathbf{K}_k$ drop. In addition, the sparsity of matrix $\mathbf{J}_k$ in Equation (13) can also be taken advantage of in order to carry out matrix multiplications with less operations (see section 3.4 in the work of Insperger and Stépán[18]). On the other hand, computational costs can be reduced further by replacing semidiscretization with more effective discretization techniques.[12-17] This changes Equation (13) only, whereas the subsequent analysis remains the same. These techniques operate with significantly smaller coefficient matrices and less matrix multiplications. Furthermore, when multiple, distributed, or time-periodic delays occur, Equation (13) should be modified only.

Apart from compatibility with other discretization techniques, the main advantage of the method is that only three constant parameters have to be determined: the bifurcation point α_{cr}, the root tendency $|\mu|'_{cr}$, and the leading coefficient $\tilde{a}_{cr}$; it is not required to compute branches of solutions point by point. Using the three constant parameters, it is possible to determine the approximate amplitude of the emerging period-1, period-2, or quasi-periodic solutions, although the amplitude is accurate in the vicinity of the bifurcation only. However, the sense (the criticality) of the bifurcation, that is, the stability of the arising solutions can also be determined based on the sign of the leading coefficient $\tilde{a}_{cr}$. According to the examples of this paper, the sign of $\tilde{a}_{cr}$ can be obtained even by a rough discretization of the solution operator, eg, by using a period resolution $p = 5$. This is typically the case when $\tilde{a}_{cr}$ is not close to zero, which makes the method a fast tool for criticality analysis.

Analyzing the criticality of bifurcations is a relevant issue in engineering. From the engineering point of view, subcritical bifurcations are considered more dangerous than supercritical ones. Unstable solutions arising from a subcritical bifurcation make the basin of attraction of the linearly stable stationary solution finite. This leads to locally but not globally stable engineering systems where oscillations may evolve due to large enough perturbations. This phenomenon is often referred to as bistability. In engineering, bistability is dangerous and must be avoided, since the designed state of the system is stable, but it may eventually lose stability to large enough external disturbances. Our future research involves engineering applications of the method presented above; for instance, the criticality of period doubling and secondary Hopf bifurcations related to milling operations can be analyzed. The regenerative machine tool vibrations in milling are described by nonlinear time-periodic DDEs, for which the phenomenon of bistability was shown to occur.[33]

ORCID

T. G. Molnar 🔟 http://orcid.org/0000-0002-9379-7121

REFERENCES

1. Hale J. *Theory of Functional Differential Equations.* New York, NY: Springer; 1977.
2. Diekmann O, van Gils SA, Lunel SMV, Walther HO. *Delay Equations: Functional-, Complex-, and Nonlinear Analysis.* New York, NY: Springer; 1995.

3. Roberts AJ. Low-dimensional modelling of dynamics via computer algebra. *Comput Phys Commun*. 1997;100(3):215-230.

4. Nayfeh AH, Mook DT. *Nonlinear Oscillations*. New York, NY: Wiley; 1979.

5. Engelborghs K, Luzyanina T, Roose D. Numerical bifurcation analysis of delay differential equations using DDE-BIFTOOL. *ACM Trans Math Softw*. 2002;28(1):1-21.

6. Breda D, Diekmann O, Gyllenberg M, Scarabel F, Vermiglio R. Pseudospectral discretization of nonlinear delay equations: new prospects for numerical bifurcation analysis. *SIAM J Appl Dyn Syst*. 2016;15(1):1-23.

7. Roose D, Szalai R. Continuation and bifurcation analysis of delay differential equations. In: Krauskopf B, Osinga HM, Galán-Vioque J, eds. *Numerical Continuation Methods for Dynamical Systems: Path Following and Boundary Value Problems*. Dordrecht, Netherlands: Springer; 2007:359-399.

8. Szalai R. Knut: A continuation and bifurcation software for delay-differential equations. http://rs1909.github.io/knut/

9. Krauskopf B, Osinga HM, Galán-Vioque J. *Numerical Continuation Methods for Dynamical Systems*. Dordrecht, Netherlands: Springer; 2007.

10. Loiseau JJ, Michiels W, Niculescu SI, Sipahi R. *Topics in Time Delay Systems: Analysis, Algorithms and Control*. Berlin, Germany: Springer; 2009.

11. Breda D, Maset S, Vermiglio R. *Stability of Linear Delay Differential Equations: A Numerical Approach with MATLAB*. New York, NY: Springer; 2014.

12. Breda D, Maset S, Vermiglio R. Pseudospectral differencing methods for characteristic roots of delay differential equations. *SIAM J Sci Comput*. 2005;27(2):482-495.

13. Breda D. Solution operator approximations for characteristic roots of delay differential equations. *Appl Numer Math*. 2006;56:305-317.

14. Butcher EA, Bobrenkov OA. On the Chebyshev spectral continuous time approximation for constant and periodic delay differential equations. *Commun Nonlinear Sci Numer Simul*. 2011;16(3):1541-1554.

15. Khasawneh FA, Mann BP. A spectral element approach for the stability of delay systems. *Int J Numer Methods Eng*. 2011;87(6):566-592.

16. Vyasarayani CP, Subhash S, Kalmár-Nagy T. Spectral approximations for characteristic roots of delay differential equations. *Int J of Dyn Control*. 2014;2(2):126-132.

17. Lehotzky D, Insperger T. A pseudospectral tau approximation for time delay systems and its comparison with other weighted-residual-type methods. *Int J Numer Methods Eng*. 2016;108(6):588-613.

18. Insperger T, Stépán G. *Discretization for Time-Delay Systems: Stability and Engineering Applications*. New York, NY: Springer; 2011.

19. Guckenheimer J, Holmes P. *Nonlinear Oscillations, Dynamical Systems, and Bifurcations of Vector Fields*. New York, NY: Springer; 1983.

20. Kuznetsov YA. *Elements of Applied Bifurcation Theory*. New York, NY: Springer; 1998.

21. Farkas M. *Periodic Motions*. New York, NY: Springer; 1994.

22. Zhang L, Stépán G. Exact stability chart of an elastic beam subjected to delayed feedback. *J Sound Vib*. 2016;367:219-232.

23. Morrison TM, Rand RH. 2:1 Resonance in the delayed nonlinear Mathieu equation. *Nonlinear Dyn*. 2007;50(1-2):341-352.

24. Ng L, Rand RH. Bifurcations in a Mathieu equation with cubic nonlinearities. *Chaos Solit Fractals*. 2002;14(2):173-181.

25. Ng L, Rand RH. Bifurcations in a Mathieu equation with cubic nonlinearities: part II. *Commun Nonlinear Sci Numer Simul*. 2002;7(3):107-121.

26. Zounes RS, Rand RH. Subharmonic resonance in the non-linear Mathieu equation. *Int J Nonlinear Mech*. 2002;37(1):43-73.

27. Ramani DV, Keith WL, Rand RH. Perturbation solution for secondary bifurcation in the quadratically-damped Mathieu equation. *Int J Nonlinear Mech*. 2004;39(3):491-502.

28. Pandiyan R, Sinha SC. Analysis of time-periodic nonlinear dynamical systems undergoing bifurcations. *Nonlinear Dyn*. 1995;8(1):21-43.

29. Butcher EA, Sinha SC. Symbolic computation of local stability and bifurcation surfaces for nonlinear time-periodic systems. *Nonlinear Dyn*. 1998;17(1):1-21.

30. Butcher EA, Sinha SC. Normal forms and the structure of resonance sets in nonlinear time-periodic systems. *Nonlinear Dyn*. 2000;23(1):35-55.

31. Sinha SC, Redkar S, Butcher EA. Order reduction of nonlinear time periodic systems using invariant manifolds. *J Sound Vib*. 2005;284(3-5):985-1002.

32. Insperger T, Stépán G. Stability chart for the delayed Mathieu equation. *Proc Royal Soc A Math Phys Eng Sci*. 2002;458(2024):1989-1998.

33. Dombóvári Z, Stépán G. On the bistable zone of milling processes. *Philos Trans Royal Soc A Math Phys Eng Sci*. 2015;373(20140 409):17.

APPENDIX

MATHEMATICA CODE

```
Quit;

(*PARAMETERS*)

a1=0.1; delta=0.7; epsi=1.; tau=2.*Pi; mu=0.5;
(*Select the bifurcation parameter and give its estimation at the bifurcation*)
b0=par; parst=-0.2;

(*PERIOD AND SEMIDISCRETIZATION STEP*)

(*time period*)
T=2.*Pi;
(*period resolution*)
p=10;
(*time step*)
dt=T/p;
(*delay resolution*)
r=IntegerPart[Chop[tau/dt]];

(*SYSTEM DEFINITION*)

(*state vector*)
u[i_]={x[i],xdot[i]};
(*system dimension*)
n=Length[u[i]];
(*determine amplitude of orbits in terms of the j-th state*)
jj=1;
(*set of linear coefficient matrices*)
DD[par_]=Table[{{0,1},
{-(delta+epsi*(Sin[(i+1)*dt]-Sin[i*dt])/dt),-a1}},{i,0,p-1}];
(*set of retarded coefficient matrices*)
EE[par_]=Table[{{0,0},{b0,0}},{i,0,p-1}];
(*set of nonlinear terms*)
g[par_]=Table[{0,-mu*Power[x[i],3]},{i,0,p-1}];

(*SEMIDISCRETIZED SYSTEM MATRICES*)

PP[par_]=MatrixExp[#*dt]&/@DD[par];
R0[par_]=MapThread[Dot,{Inverse/@DD[par],EE[par]}]+
1/dt*MapThread[Dot,{((Inverse[#].Inverse[#])&/@DD[par]-
(tau-(r-1)*dt)*Inverse/@DD[par]),
(IdentityMatrix[n]-#)&/@PP[par],EE[par]}];
R1[par_]=-MapThread[Dot,{Inverse/@DD[par],EE[par]}]+
1/dt*MapThread[Dot,{(-(Inverse[#].Inverse[#])&/@DD[par]+
(tau-r*dt)*Inverse/@DD[par]),
(IdentityMatrix[n]-#)&/@PP[par],EE[par]}];
h[par_]=MapThread[Dot,{(#-IdentityMatrix[2])&/@PP[par],
Inverse/@DD[par],g[par]}];
(*augmented state vector*)
z=Table[Flatten[Table[u[i-k],{k,0,r}]],{i,0,p-1}];
```

```
(*linear part of map*)
JJ[par_]=Table[Join[ArrayFlatten[{{PP[par][[i+1]],
Table[0,{n},{(r-2)*n}],R1[par][[i+1]],R0[par][[i+1]]}}],
ArrayFlatten[{{IdentityMatrix[r*n],Table[0,{r*n},{n}]}}]],{i,0,p-1}];
(*nonlinear part of map*)
H[par_]=MapThread[Join,{h[par],Table[0,{p},{r*n}]}];


(*BIFURCATION POINT*)


II=IdentityMatrix[Last[Dimensions[JJ[par]]]];
(*linear map as function of the bifurcation parameter*)
AApar[par_?NumberQ]:=Nest[{#[[1]]+1,Chop[JJ[par][[#[[1]]+1]].#[[2]]]}&,
{0,II},p][[2]];
(*corrected bifurcation point*)
parst=par/.FindRoot[Abs[Eigenvalues[AApar[par],1]]-1,
{par,parst}];
(*map at bifurcation point*)
JJst=Chop[JJ[parst]];
Hst=Chop[H[parst]];


(*DEFINITION OF <.,.,.> AND <.,.,.> PRODUCTS*)


(*<.,.,.> product between third and second order matrices*)
ThreeTwoProduct[X_,Y_,Z_]:=Transpose[Transpose[
X,{1,3,2}].Y,{1,3,2}].Z;
(*<.,.,.> product between third and third order matrices*)
ThreeThreeProduct[X_,Y_,Z_]:=Transpose[Transpose[
X,{1,3,2}].Y,{1,4,2,3}].Z;
(*<.,.,.> product between fourth and second order matrices*)
FourTwoProduct[X_,Y_,Z_,W_]:=Transpose[Transpose[Transpose[
X,{1,4,2,3}].Y,{1,4,2,3}].Z,{1,4,2,3}].W;


(*RESULTANT MAP*)


(*LINEAR PART*)
(*matrices Q_{j-1,0}*)
Mj=NestList[{#[[1]]+1,Chop[JJst[[#[[1]]+1]].#[[2]]]} &,
{0,II},p-1][[All,2]];
(*matrices Q_{p-1,j+1}*)
Nj=Reverse[NestList[{#[[1]]-1,Chop[#[[2]].JJst[[#[[1]]-1]]]} &,
{p+1,II},p-1][[All,2]]];
(*matrix A*)
AA=Chop[JJst[[p]].Mj[[p]]];


(*QUADRATIC PART*)
Kj=(D[#[[1]],{#[[2]]},{#[[2]]}]/.Thread[#[[2]]->0]) &/@
(Transpose[{Hst,z}]);
(*<K_j,Q_{j-1,0},Q_{j-1,0}>*)
KMMj=MapThread[ThreeTwoProduct,{Kj,Mj,Mj}];
(*matrix B*)
BB=Total[MapThread[Dot,{Nj,KMMj}]];
```

```
(*CUBIC PART*)
Lj=(D[#[[1]],{#[[2]]},{#[[2]]},{#[[2]]}]/.Thread[#[[2]]->0]) &/@
(Transpose[{Hst,z}]);
(*<L_j,Q_{j-1,0},Q_{j-1,0},Q_{j-1,0}>*)
LMMMj=MapThread[FourTwoProduct,{Lj,Mj,Mj,Mj}];
(*matrices Subscript[Q,j-1,l+1]*)
Qjl=Table[Reverse[NestList[{#[[1]]-1,Chop[#[[2]].JJst[[#[[1]]-1]]]} &,
{j+1,II},j-1][[All,2]]],{j,1,p-1}];
(*Sum(Q_{j-1,l+1}<K_l,Q_{l-1,0},Q_{l-1,0}>)*)
QKMMj=Join[{0.*KMMj[[1]]},Total[MapThread[
Dot,{#,KMMj[[1;;Length[#]]]}]]&/@Qjl];
KQKMj=(MapThread[ThreeThreeProduct,{Kj,QKMMj,Mj}]+
MapThread[ThreeTwoProduct,{Kj,Mj,QKMMj}])/2.;
(*matrix \tilde{C}*)
CCt=Total[MapThread[Dot,{Nj,LMMMj}]]+3.*Total[MapThread[Dot,{Nj,KQKMj}]];
(*matrix C*)
CC=1/6*Total[Transpose[CCt,#]&/@(Prepend[#,1]&/@Permutations[{2,3,4}])];


(*RELEVANT EIGENVALUES AND EIGENVECTORS*)

sec=SessionTime[];
eigs=Eigensystem[AA,2];
theta0=Arg[eigs[[1,1]]];
(*critical eigenvalue*)
mu0=Exp[I*theta0]//Chop;
(*critical right eigenvector*)
qq=eigs[[2,1]]//Chop; eigsT=Eigensystem[Transpose[AA],2];
(*critical left eigenvector*)
pp=If[Im[mu0]==0,eigsT[[2,1]],eigsT[[2,2]]]//Chop;
(*normalization of eigenvectors*)
pp /= Conjugate[Conjugate[pp].qq]//Chop;
(*type of bifurcation*)
If[Im[mu0]==0,If[mu0>0,Print["Nongeneric fold (pitchfork) bifurcation"],
Print["Flip bifurcation"]],Print["Neimark-Sacker bifurcation"]]
StringJoin["Bifurcation point: ",ToString[parst]]


(*ROOT TENDENCY*)

sec=SessionTime[];
(*command for matrix adjoint*)
Adj[m_]:=Map[Reverse,Minors[Transpose[m],Length[m]-1],{0,1}]*
Table[Power[-1,i+j],{i,Length[m]},{j,Length[m]}];
(*A'cr*)
AAp0=Total[MapThread[Dot,{Nj,Derivative[1][JJ][parst],Mj}]];
(*mu'cr*)
mup0=-Tr[Adj[mu0*II-AA].(-AAp0)]/Tr[Adj[mu0*II-AA]];
(*|mu|'cr*)
s0=(Re[Conjugate[mu0]*mup0]/Abs[mu0])//Chop;
StringJoin["Root tendency: ",ToString[s0]]
```

```
(*LEADING COEFFICIENT*)

sec=SessionTime[];
(*leading coefficient acr*)
a00=If[Im[mu0]==0,If[mu0>0,
(*fold*)
1/6*pp.CC.qq.qq.qq-1/2*pp.BB.qq.
(LinearSolve[Append[Flatten/@Thread[{AA-II,qq}],Join[pp,{0}]],
Join[BB.qq.qq-(pp.BB.qq.qq) qq,{0}]][[1;;-2]]),
(*flip*)
    -(1/6*pp.CC.qq.qq.qq-1/2*pp.BB.qq.Inverse[AA-II].BB.qq.qq)],
(*Neimark-Sacker*)
1/2*Re[Exp[-I*theta0]*(Conjugate[pp].CC.qq.qq.Conjugate[qq]+
2*Conjugate[pp].BB.qq.Inverse[II-AA].BB.qq.Conjugate[qq]+
Conjugate[pp].BB.Conjugate[qq].
Inverse[Exp[2*I*theta0]*II-AA].BB.qq.qq)]];
(*scaled leading coefficient \tilde{a}cr*)
a0=If[Im[mu0]==0,a00/Max[Power[Table[qq[[jj+m*n]],{m,0,r}],2]],
a00/(4*Max[Power[Abs[Table[qq[[jj+m*n]],{m,0,r}]],2]])];
StringJoin["Leading coefficient: ",ToString[a0]]

(*BIFURCATION DIAGRAM*)

plotopts={PlotRange->{{-1,1},{0,1}},AxesOrigin->{0,0},
PlotStyle->{Blue},Frame->True,FrameLabel->{"parameter","amplitude"},
FrameStyle->Directive[FontSize->16],PlotRangePadding->None,
AspectRatio->1,ImageSize->400};
Plot[{Sqrt[-s0*(par-parst)/a0]},{par,-1.5,1.5},Evaluate@plotopts]
```